MASS FABRICATION & EVOLUTION OF BEADS ON FIBER

by

KIRTHIKA SURESH

Presented to the Faculty of the Graduate School of

The University of Texas at Arlington in Partial Fulfillment

of the Requirements

for the Degree of

MASTER OF SCIENCE IN MECHANICAL ENGINEERING

THE UNIVERSITY OF TEXAS AT ARLINGTON

MAY 2018

Acknowledgements

I am honored to work with Dr. Cheng Luo, my thesis advisor and committee chair, whom I idolize and respect. His knowledge and expertise are immensely valuable, especially in the field of Micro/Nanofabrication systems. I truly thank him for giving me this research opportunity. His selfless guidance and patience are his most precious gifts to me.

My sincere thanks to Dr. Hyejin Moon and Dr. Zhen Xue Han, my thesis committee members, for taking time out of their schedule and being a part of the thesis committee and for giving their useful insights on my work.

Utmost thanks and appreciation to my research colleagues, Mr. Manjarik Mrinal, Mr. Xiang Wang and Dr. Zhihai Jia, also to my dear friends Mr. Anish Ganta and Ms. Sravya Sasetty for being the key sources of support.

I am forever in debt to my family; my father Mr. Suresh Raghuramarao, my mother Mrs. Sujatha Thamada and my dear Sister Ms. Sai Pooja Suresh for believing in me and making my dreams their own. Their unceasing love, care, sacrifice and moral support is the reason for who I am on this day.

May 1, 2018

Abstract

MASS FABRICATION & EVOLUTION OF BEADS ON FIBER

Kirthika Suresh, M.S.

The University of Texas at Arlington, 2018

Supervising Professor: Cheng Luo

In this work, we systematically explore the relation between the coating speeds and the finally formed liquid beads on fiber. The main focus of the paper lies with contact angle, length and height of beads on fiber and the fiber drawing velocity. For this purpose, free energy variation method is applied, based upon which the boundary conditions for the beads-on-fiber system and governing equations were re-derived. A combination of both, first and the second kind of the Legendre's elliptical functions are used to determine the geometrical shape of the beads. Contact angle is extracted from the experimental data by using a semi-analytic approach. This approach can be referred to for determining surface tension of fluids for cases such as sessile drop on a fiber.

Table of Contents

List of Illustrations

List of Tables

Chapter 1 INTRODUCTION

Formation of liquid beads on a fiber is shown in nature through the simple example of spider. A spider produces a sticky cylindrical coating over its web while producing it. This layer of cylindrical film coating is then split into several micro-beads due to the instability phenomenon directly resulting in bulging of the sticky material at certain distances. It is said to be observed that the beads are triple the size after every three beads thereby creating a pattern of beads on the web. The spider forms this structure as a trap for the flies and other prey[1].

We are trying to understand the formation of beads on a fiber by a method which can produce a large number of beads in a controlled manner with specific bead sizes and spacings. Therefore, in our case, the sticky material, such as in the spider situation, is replaced by silicone oil and the web-like material here is copper wire for experimental analysis.

Chapter 2 LITERATURE

Several previous studies show us the process of coating of a fluid over a thread-like, cylindrical filament in controlled conditions, explaining the various factors that affect the bead formation over the fiber surface.

Experiments[2] were conducted to deposit a stream of molten wax with a method called sweep deposition wherein the molten wax is deposited on a cold solid substrate to acquire molten wax beads. The solidification can be carried out via various means such as thermal, chemical or photochemical processes. The instability and wavelength conditions were predicted for the wax beads[3]. The rate of solidification of molten material is slower when compared to the rate of instability, which increases rapidly, resulting in bead non-uniformity. Contact line arrest is claimed to be the prerequisite for bead formation, at least in the case of the liquid droplets.

Another study[4] explains the film thickness of liquid that is entrained on a fiber drawn out of a fluid bath by both slow and quick coatings. There are several geometries of solids which can be used for fluid coating methods, Landau, Levich, Derjaguin (LLD) theory serves as a tool for this. Previous works on geometries such as plate, roll, emptying of the capillary tube and other such complicated geometries were all mentioned. A well-defined parameter for studies related to fiber is the fiber radius, which, according to the author, allows isolating

effects from each other. The fiber is drawn at high velocities out of the complex liquid bath to be coated.

A traditional way of film coating molten wax over a wick for candle making is a great example. A similar kind of example is the freeze-coating or hot dipping method. A thin wire is dipped into a molten metal sink and then removed out after a specified time, called the dipping time, with the metal frozen to the wire surface. An important observation is the increasing film thickness with temperature up to the same temperatures of both the molten metal and the wire after which the thickness decreases. In this case, the coating thickness is said to depend on the viscous drag and the freezing.

Some studies discuss the conditions under which the bead occurs and whether the bead formations are stable or unstable, e.g., a bulge in the film is an unstable bead. The author explains that an unstable small diameter liquid jet splits into several tiny droplets. In this paper, they show a relatively simple inviscid theory which helps in computing the wavelength that results in the maximum growth of the bead instability (small bond number) and a comparison with the dominant wavelength from the experiments. The beads formed at lower contact angles are uniform beads.[5]

A tuning fork can be used to create a frequency obeying the equation of instability, the condition originally derived by Lord Rayleigh, $\lambda \geq 2\pi a$. Similarly, two tuning forks were used to create two different

oscillations that build up with time resulting in the breakage of the jet into separate droplets. The usage of fluids which have different viscosities with time, which are highly complex liquids result in what is called the Marangoni coatings.[4]

Excess Pressure

For a liquid drop, the excess pressure is *P*.

$$P = \frac{2\sigma}{R} \quad (1)$$

A liquid drop has only one surface with surface tension σ. In the case of bubbles, there are two surfaces with $\sigma = 2f$. From this we understand that smaller radii droplets have larger excess pressure. At the film state, the radii are infinite, which makes the excess pressure difference zero across the surface.

Bond Number

Bo number consists of the capillary and gravity forces.[4]

$$Bo = \rho g r^2/\gamma = r^2\kappa^2 \quad (2)$$

When the bond number is small, the Laplace pressure is dominant over the hydrostatic pressure, and in this case the gravity force is neglected.

The target of this work also lies in producing beads on fiber on a large scale and in the most economical method[4]. In previous studies,

the dip-coating method was widely used to achieve bio-inspired periodic spindle-knots where short length fibers can only be treated by an ‘immersing-in/drawing-out' operation[1].

Firstly, the instability of the film grows, followed by the growing of the film thickness in some regions (radial extension). The instability further grows to depict that the Laplace pressure is small within the thick films when compared to the thin films.[1] This naturally leads to the breakage of the film resulting in the formation of the spindle knots.

$$\Delta P = \gamma\left(\frac{1}{R_1}+\frac{1}{R_2}\right), \tag{3}$$

Where ΔP is the excess Laplace pressure, R_1 and R_2 are the principal radii of surface curvature at a single point,[6] and γ is the interfacial tension. The above equation is universally constant. This will be our equilibrium condition, i.e., Laplace excess pressure is constant everywhere across the drop surface, and the instability of the film is due to what is called the Rayleigh Instability.

The equilibrium between the viscous forces and surface tension creates distortion in the liquid-air interface. This is the dynamic meniscus which affects the film thickness. At lower velocities the film thickness abides to the LLD theory provided. Here the dynamic meniscus is stable, and the resulting region is called the visco-capillary region. The dynamic meniscus is unstable at higher velocities, where

the effect of inertia becomes vital, thereby tending to form the visco-inertial region.

As explained in the study[5], a perturbation is created on a cylindrical film using a tuning fork if the criteria $\lambda \geq 2\pi a$ (where a is the radius of the cylindrical film). Two different perturbing oscillations result in two separate beads, which clearly explains the bead splitting concept that fulfills the criteria of each bead having a separate associated perturbing frequency.

2.1 The perturbed cylinder of liquid

As observed in a tap water flow, the cylinder does not sustain the cylindrical film and tends to break into several droplets due to the growth in the amplitude of the oscillation at the surface of the liquid jet. These oscillations decay away in a small length of the cylinder. As observed at the beginning of the water jet from a tap, a cylindrical jet is retained up to a certain length. Pressure variations are considered the main reason for these instabilities.

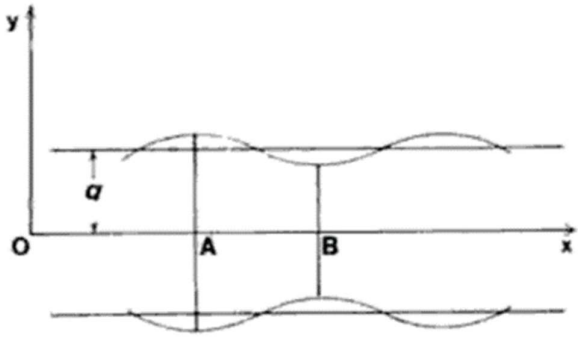

Figure 1: Perturbed Cylinder of Liquid[5]

2.1.1 How do the pressure variations affect the bead formation?

There are two things that occur during the bead formation, the radial extension and the radial contraction as explained in the phenomenon of the perturbed cylinder in reference.[5] If the pressure is higher at the region of radial extension, *A*, then some of the liquid from this region is pushed to the region which is radially contracted, *B*, to equalize the liquid distribution, making it stable. The pressure difference helps us determine the conditions of the stability and instability of the cylinder. We use the Laplace-Young equations to acquire these pressure difference values.

To acquire beads of specific sizes, we need control over the pressure variation at the radial extension and radial contraction regions. For us to achieve specific distances between each bead or number of beads in the particular length of cylindrical film, we need control over the oscillation created and its amplitude.

2.2 Transformation: Cylinder to Bead

The following figure, from an interesting study, shows the step-by-step transformation of a liquid cylinder into spheres.[7]

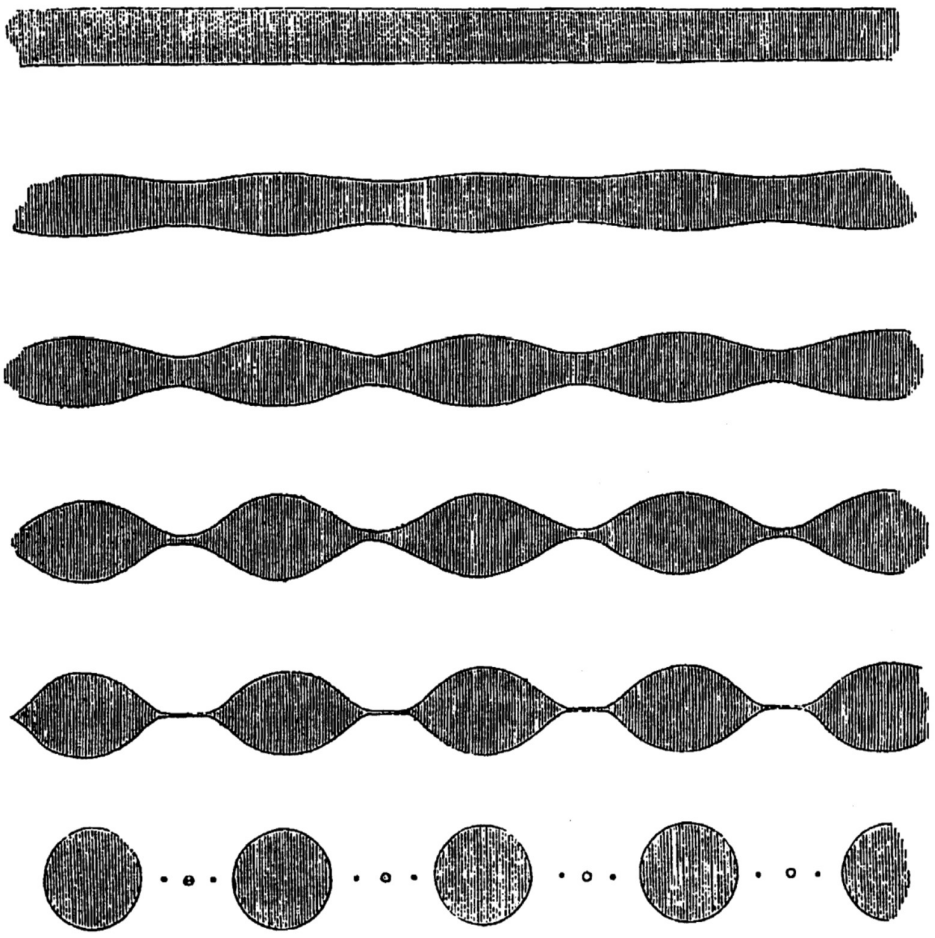

Figure 2: Liquid cylinder to beads transformation[7]

When a liquid drop loses its cohesive interactions upon contacting a surface, it is no more in its “happy state”. This why liquid tends to adjust its shape to its convenience - the state of interactions with its neighbors. Minimal surface interaction and more neighbor

interaction is what we observe in the case of bead formation from breakage of the film; this state is called the “happy state.”[8]

(i) Smaller drops have higher pressure. To attain an equilibrium state, the higher pressure drop must combine with lower the pressure drop. This phenomenon occurs in an oil-water emulsion and is called Ostwald's ripening.[8]

(ii) It was observed that the liquid cylinder tends to lower its surface energy by converting itself into droplets. The amplified wavelength that exceeds the perimeter of the liquid cylinder results in its breakage into tiny droplets. Perturbations grow to compel the jet breakage into droplets.

(iii) If at all one wonders about the calculation of the sizes of these tiny droplets, Lord Rayleigh's explanation of the fast distortion mode is to be familiarized.

It is mentioned that the perturbations grow downstream leading to the resultant droplet formation. Many early works explain that the subsequent contraction for bead formation is due to capillary force.

2.3 Causes of Deviation

(i) Effects related to interfacial regions of solid/liquid at lower velocities and gravity.

(ii) Inertia effects at fast fiber withdrawals, because the boundary conditions at the solid/liquid interface are responsible for the liquid entrainment. Hence, interfaces play a crucial role.

(iii) liquid/gas interfacial effects for complex fluid coatings, e.g., soap water or emulsions.[4]

One important observation from a study explain their results achieved on the variation of the solution concentration. On increasing the weight percentage, the V_{cr} value decreases below which the film coating is uniform over the fiber. When $V > V_{cr}$ the coating is thicker and thus breaks to obtain the spindle-knot structures.[1]

In previous works, the microcrystalline wax and Plexiglas target were used for the study.[5] The factors that affected the fiber coatings were mainly the capillary pressure, substrate withdrawal speed,[6] density, viscosity and surface tension.

2.3.1 Capillary Pressure

The pressure difference at the interfaces of the two immiscible fluids due to the capillary forces, such as the surface tension and the interfacial tension forces, is the capillary pressure.

2.3.2 Surface Tension

Studies[5] express the behavior of the molecules of the liquid at positions such as exterior/on the surface and interior, like the

discussion in the reference[9] according to their research on previous studies. The molecules at the bulk of the fluid experience the forces from all directions giving a resultant force of zero, over a macroscopic time. Molecules are said to experience more force at the surface when the above region is fluid when compared to the gaseous region since the fluid density is higher than that of the gaseous density. Therefore, a pulling force is experienced by the molecules in such situations. The author indicates that this pulling force reduces the surface area. For example, the moles of water in this layer can transform into a water droplet of a spherical shape. Additional effects on density are also mentioned which are not of our focus. The surface tension is visible on these layers of molecules, i.e. the force per unit length in a liquid-vapor interface. Surface tension has different denotations at different phase interactions such as Interfacial Tension, Adhesion Tension and so on.

Three surface tension forces are visible at the line of contact of the three phase system: σ_{sl} between solid and liquid phases toward the contact angle, σ_{lg} between the liquid and gas phases and σ_{sg} between the solid and gas phases.[5]

2.3.3 Contact Angle

Contact Angle is measured as an angle between the meeting point of the solid surfaces and the tangent planes of the liquid, contacting at a fixed angle along their line of contact.

This parameter is usually measured by taking a side view – a photograph of the droplet on a solid surface – and by measuring the angle using a protractor tool. One other method is to measure by optical reflection technique for more accuracy in smaller beads. Several other techniques were used for manual measurement of this particular parameter.

2.4 Bead Formation Process

Some studies that carried out experiments with beads on a fiber explain the step-by-step process of bead formation. The author has explained that the beads form initially by pinching at their necks, where the film is thinner than that of the initial film formed. As the thinning increases it forms a bead.[10]

Chapter 3 MATHEMATICAL MODEL

Consider a bead on a fiber. The wire surface may be smooth/ rough and wetting/non-wetting. *a* and *b* points are the triple contact points[11] on the side of the fiber surface, curve '*ab*' is assumed as a circular arc of radius '*R'* and is represented as a meridian curve of the bead (Fig. 5). Let *H* and *L*, respectively, denote the thickness and base length of the drop. Use r_o to represent the radius of the fiber. Set *θ* to be equilibrium contact angle. Then, by geometric analysis, we have

$$L = 2Rsin\theta, \tag{4}$$

$$H = R(1 - cos\theta). \tag{5}$$

Set a rectangular *x-y* coordinate system for a drop, as defined in Fig. 5. The volume of a drop, *V*, can be expressed as:

$$V = \pi \int_{-L/2}^{L/2} y^2 dx - \pi {r_o}^2 L. \tag{6}$$

The first term on the right-hand side in eqn (6) denotes the total volume of a drop along with the fiber that is underneath it. Whereas, the second term is the volume of the fiber. With the help of Eq. (4), it follows from Eq. (6) that

$$V = 2\pi[-\frac{R^3 sin^3\theta}{3} + R^2 sin\theta(R - r_o cos\theta) + R^2(r_o\theta - R\theta cos\theta)] \tag{7}$$

In addition, V can also be expressed by

$$V = \pi (r_o+e)^2 \lambda^* - \pi \lambda^* r_o^2. \quad (8)$$

here

$$e \approx r_0 Ca^{2/3}, [8] \quad (9)$$

$$Ca = \eta u/\gamma, \quad (10)$$

$$\lambda^* = 2\sqrt{2}\pi r_o = 8.9 r_o .[8] \quad (11)$$

In Eq. (10), η, u, and γ are viscosity, fiber withdrawing speed, and surface tension, respectively. Eq. (12) holds true only in the limit $e<<r_o$. The distance between the centers of two neighboring drops is λ^*, which is given in Eq. (11). Long time ago, it was very well understood by Rayleigh that for kinetic reasons, the particular wavelength λ^* wins out.[8] It is the wavelength that grows faster than all the possible unstable wavelengths. Thus, it is the critical wavelength that makes a film break into drops. Substitution of Eqs. (7)-(11) into Eq. (7) results in an equation in the form of

$$V_o(u)=F(R). \quad (12)$$

3.1 Solution Procedure

Measure θ and r_o. For given u, R can be determined by solving Eq. (9). Furthermore, with the aid of Eqs. (4) and (5), u-L and u-H relations can be found.

In addition, the spacing between the centers of two neighboring drops is λ^*, which is given in Eq. (11).

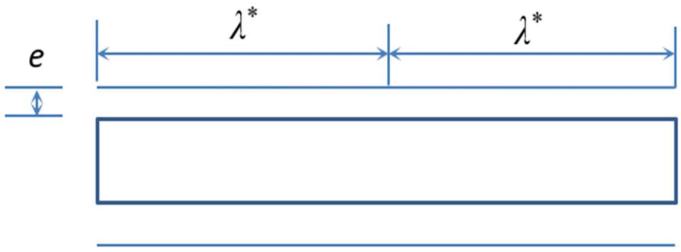

Figure 3: Cross-sectional view of a liquid film coated on a fiber

Figure 4: The liquid film loses stability due to disturbance

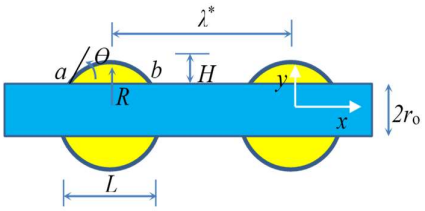

Figure 5: The liquid drops finally formed due to instability of the film

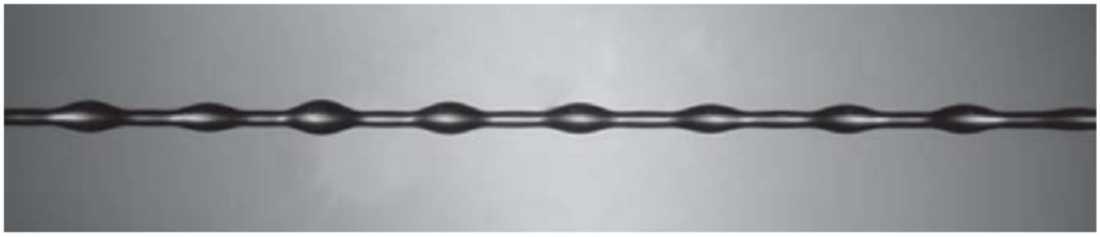

Figure 6: Finally formed drops[8]

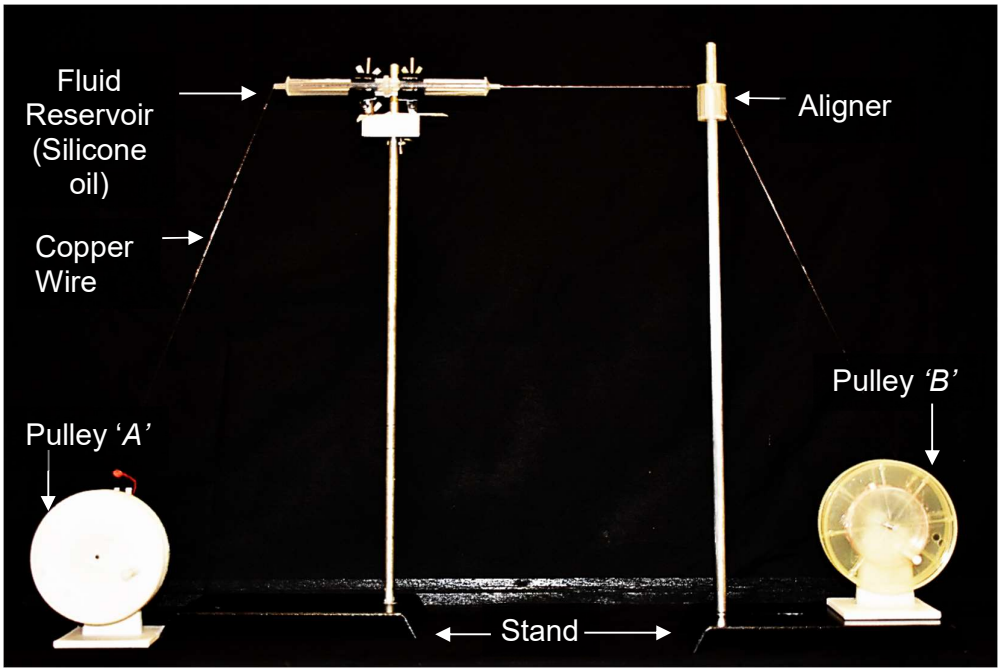

Figure 7: Experimental Set-up

The picture portrays the experiment set-up for the horizontal film coating on a fiber. The pulley '*A*' is initially coiled of copper wire, thickness($2r_o$) of 0.08mm. The pulley *'A'* also has some additional add-ons, i.e., the thread loop which helps in maintaining the alignment of the thread, then the grip adjuster-which helps keep the thread taut, this is placed right behind the pulley, beneath the rotating axle. Next in the set-up is the fluid reservoir which was made using two syringe barrels, attached to their bottoms, a slit is made on the top of this barrels so as to fill in the liquid, here silicone oil (η=45-55 mm^2/s @ 25^oC)[12], from time to time. Following this, we have an aligner placed horizontally to

the reservoir and is fixed to the stand. Then we have the pulley '*B*', this is used to manually rotate at various speeds, in our experiment we have three range of speeds based on which we achieve beads of three different size ranges, hence we categorized them into three groups namely the small beads, medium beads and big beads. A light source is usually placed behind the set-up while recording the bead formation, this recording is done using the high-speed camera placed facing this whole set-up and is focused at the right tip of the reservoir to observe the micro-beads.

As previously seen in the experimental set-up, the fiber is drawn through the liquid reservoir using pulley *'B'*. We manually rotate the pulley *'B'* at several different velocities beginning from no velocity to highest velocity. In the case, at *v=0*, we get no film. As the velocity is made to 1 cm/s or less we observe fluid deposition on the fiber, but very thin coating, this film does not split into beads since the speed of fiber drawn is so small for it to create a film instability that can result in bead formation.

In some studies mentioned in a reference[4], the authors focus upon the dynamic contact angle which is at the exit region of the liquid bath and beginning of the fiber withdrawal but our main attention is toward the beads and the various stages of their formation.

4.1 Categorization of Beads

The withdrawal of fiber from reservoir, in our experiment, was differentiated into three different stages for better understanding of the beads and the study of their formation. This is done by withdrawing the fiber at different ranges of velocities such as explained in the followed cases:

4.1.1 Small Beads

In this case, the pulley '*B*' is rotated very slowly within the velocity range of 3.169-4.500 cm/s, since it is manually driven, care is taken to maintain the uniform velocity. The beads are symmetrical about the fiber axis. The total height (H_1 in mm) and length (L in mm) of the beads range between the range 0.127-0.186mm and 0.282-0.382 respectively.

4.1.2 Medium Beads

The fiber drawing velocity for the medium beads range between 16.97-21.40 cm/s. The total height (H_1 in mm) and length (L in mm) of the beads range between the range 0.435-0.859mm and 0.679-1.088mm respectively.

4.1.3 Big Beads

When the fiber drawing velocity ranges from 36.76-39.45cm/s we achieve big beads. Here the film breaks to form a bead within 0.065s. The bead appears to be hinged such that it allows most of its volume to lie at the bottom portion of the bead, hence are clearly unsymmetrical about their fiber axis. The total height (H_1 in mm) and length (L in mm) of the beads range between the range 0.95-0.96mm and 1.10-1.11mm respectively.

After every trial experiment of fiber withdrawal, as soon as the fiber is made to halt we observe the beads to be dynamic in nature, in search of their most stable position.

Chapter 5 RESULTS

5.1 Case I : Small Bead Formation (*v*=3.3 cm/s)

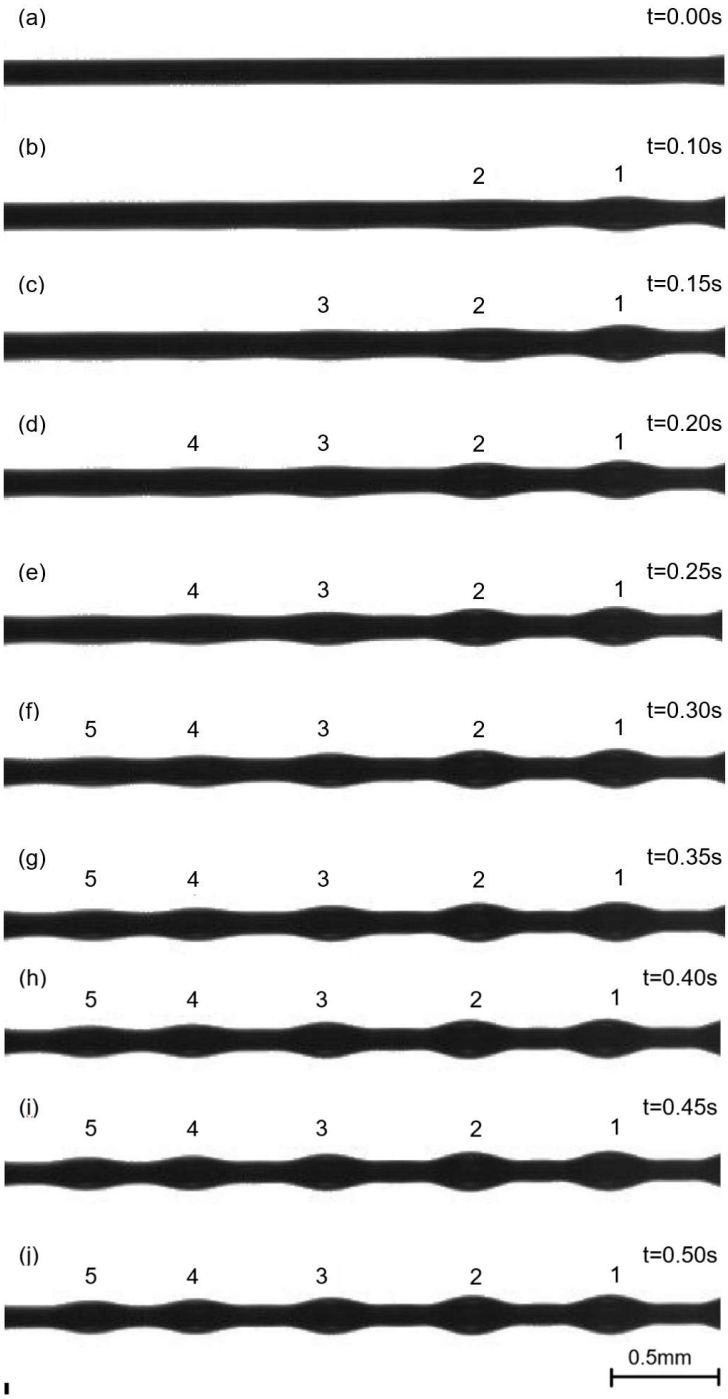

Figure 8: Evolution of Small Beads

(i) In figure 8(a), the fiber is horizontally drawn from the fluid reservoir at a velocity of 3.3 cm/s and is brought to a stop, at t=0.00s. A very thin coating of the silicone oil forms over the copper wire.

(ii) In figure 8(b), at t=0.10s, the pinching process begins over the film. The film bulges into a spindle-knot shape. The oscillation responsible for the formation of primary bead, this oscillation continues to increase in amplitude to form secondary bead.

(iii) In figure 8(c), the primary bead increases in volume due to further pinching of the neck region. Whereas the secondary beads evolve in the same way.

(iv) In figure 8(d), primary beads have completely evolved. Same procedure is seen in the following beads.

(v) Figures 8(e) to 8(i) show the time steps of the development of the beads.

(vi) In figure 8(j), we achieve the fully evolved small beads.

5.2 Case II : Medium Bead Formation (v=16 cm/s)

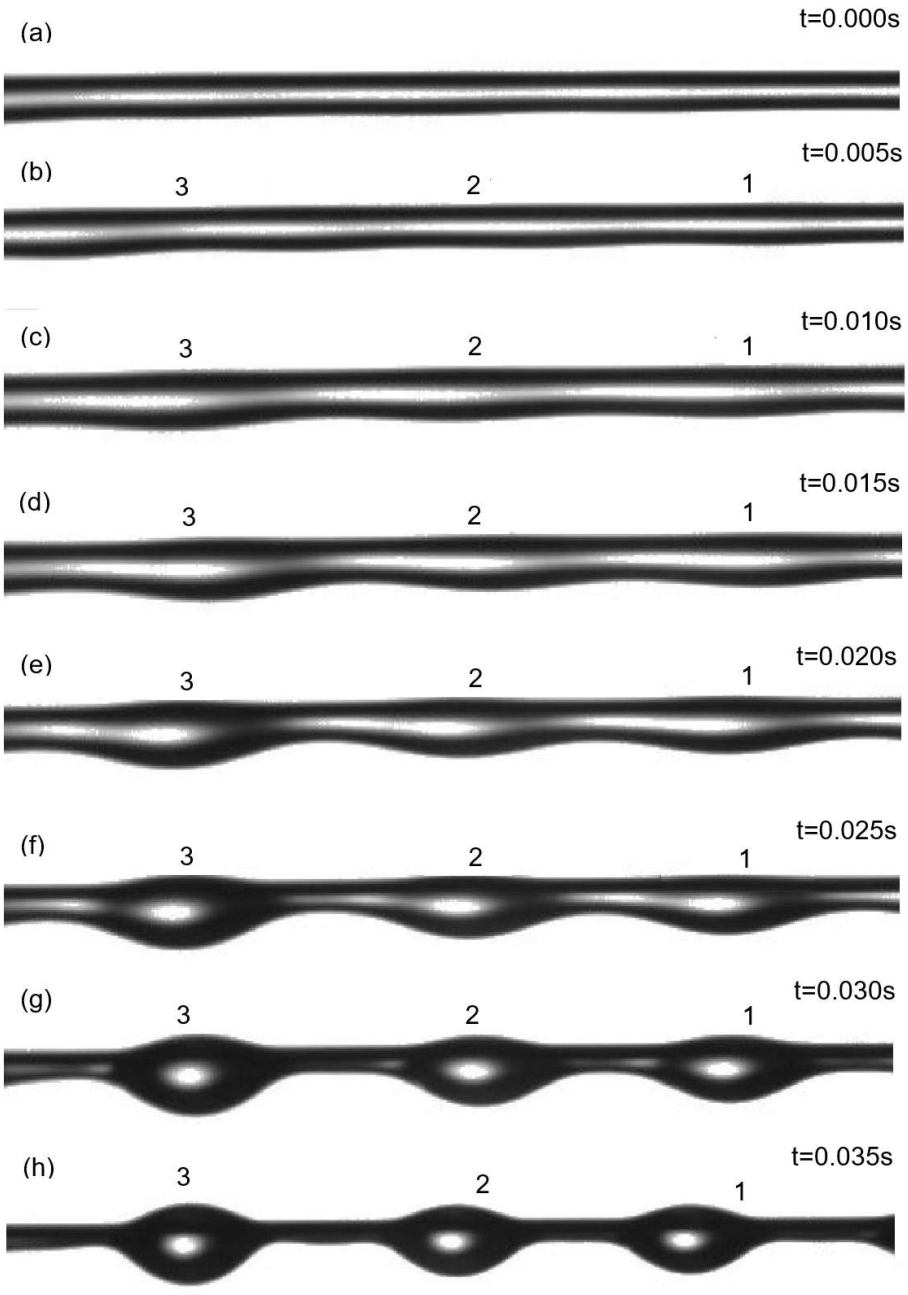

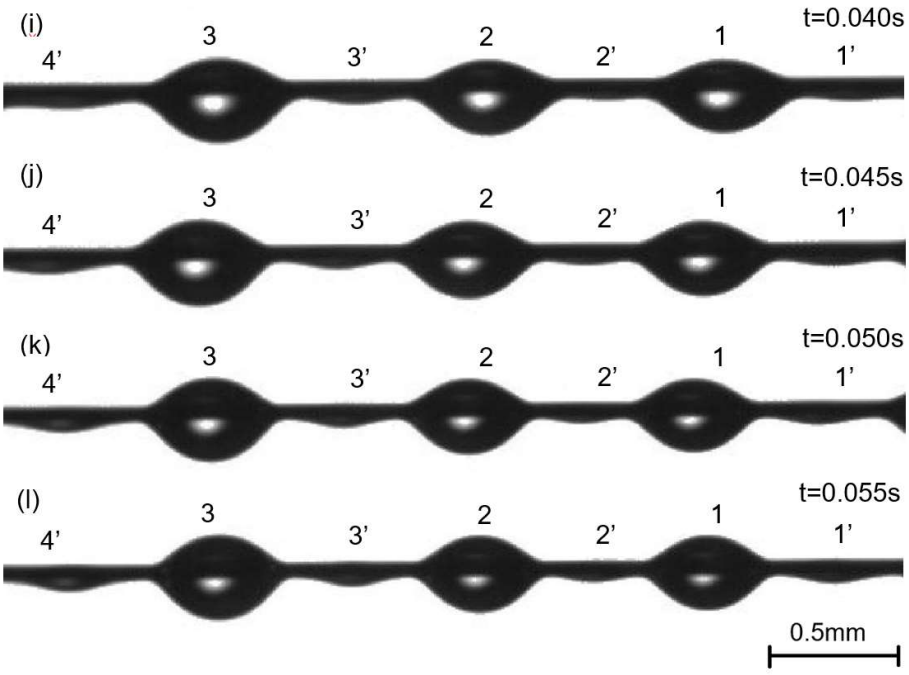

Figure 9: Evolution of Medium Beads

(i) Figure 9(a), at *t*=0.000s, shows the fluid film coating of silicone oil formed upon the copper wire, horizontally drawn at 16 cm/s. It is noticed that the thickness of the fluid coating on the fiber is thicker than the small beads case. This gives us a live observation that, “film thickness increases as the fiber drawing velocity is increased”.

(ii) Figure 9(b), at *t*=0.005s, shows the primary, secondary and tertiary beads (beads 1, 2 and 3) where all of these beads develop a very minute curvature, this is due to the pinching at the neck, mainly because of the instability created by the oscillation that occurs during

the fiber withdrawal. This is sufficient to create variations in pressure as explained earlier in the introduction.

(iii) Continuing to figure 9(c) where we observe increment in the curvature is visible.

(iv) In figure 9(d), the beads begin to accumulate more liquid from their film region by consequent film pinching at the neck region to upgrade themselves as that seen in the figure 9(e).

(v) Figures 9(f) to 9(h) depict the extremely thin neck region this allows them to form the fully formed medium beads.

(vi) As the medium beads are shaping up the left-over film deposit recoil and feed to develop on either side of the primary beads. Hence, now we get, '*satellite beads*', labelled as 1', 2', 3' and so forth in this study, as seen in the figures 9(i) to 9(l).

Note that the labelling is done from the right to the left, in the manner of 'first-come-first-serve' basis.

(vii) It is believed in our study that the satellite beads form at the midway to its next bead if the fiber-drawing velocity is maintained to be uniform.

(viii) Finally, figure 9(l) shows the fully formed *medium beads* along with their *satellite beads*.

5.3 Case III : Big Beads Formation (*v*=35 cm/s)

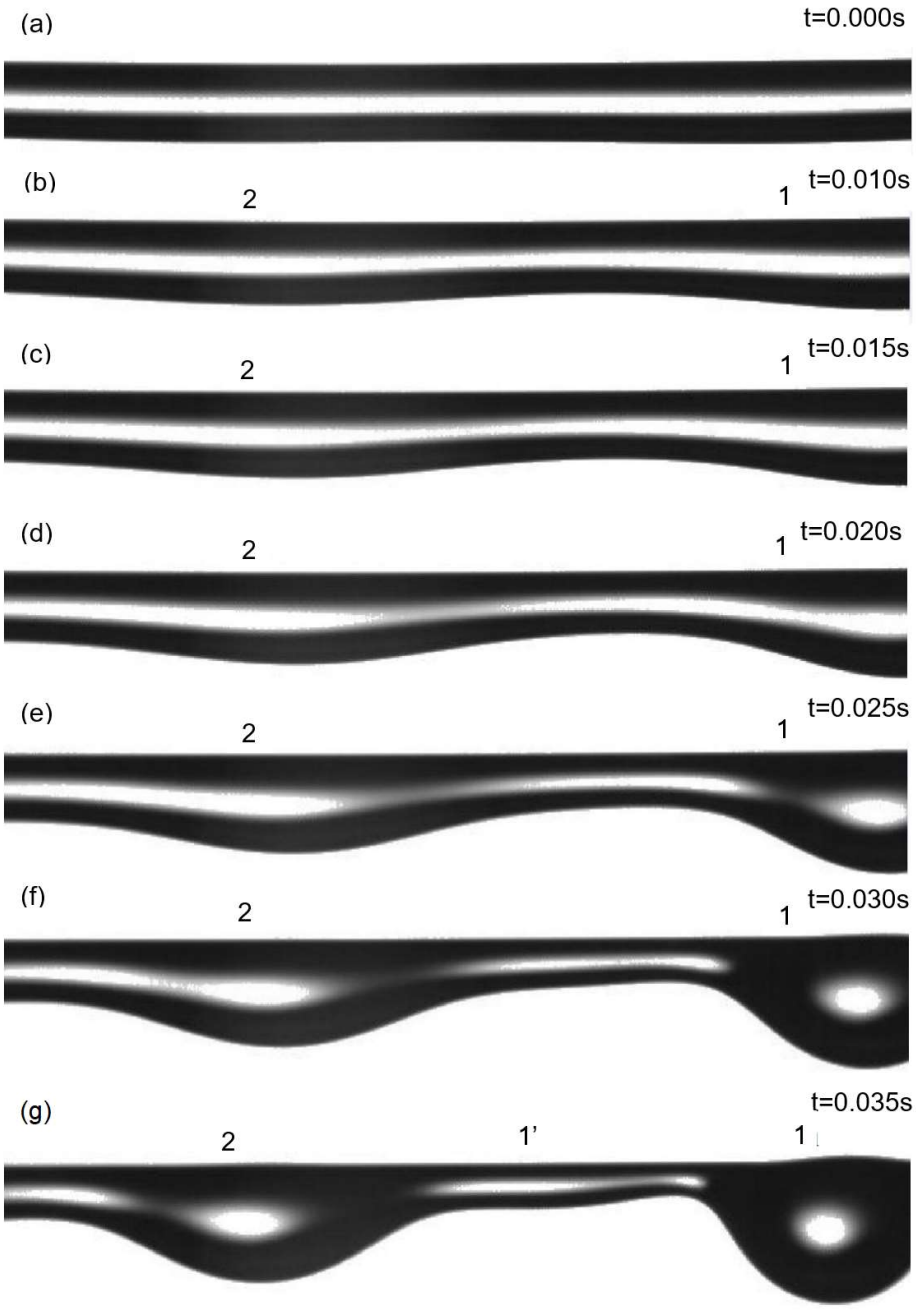

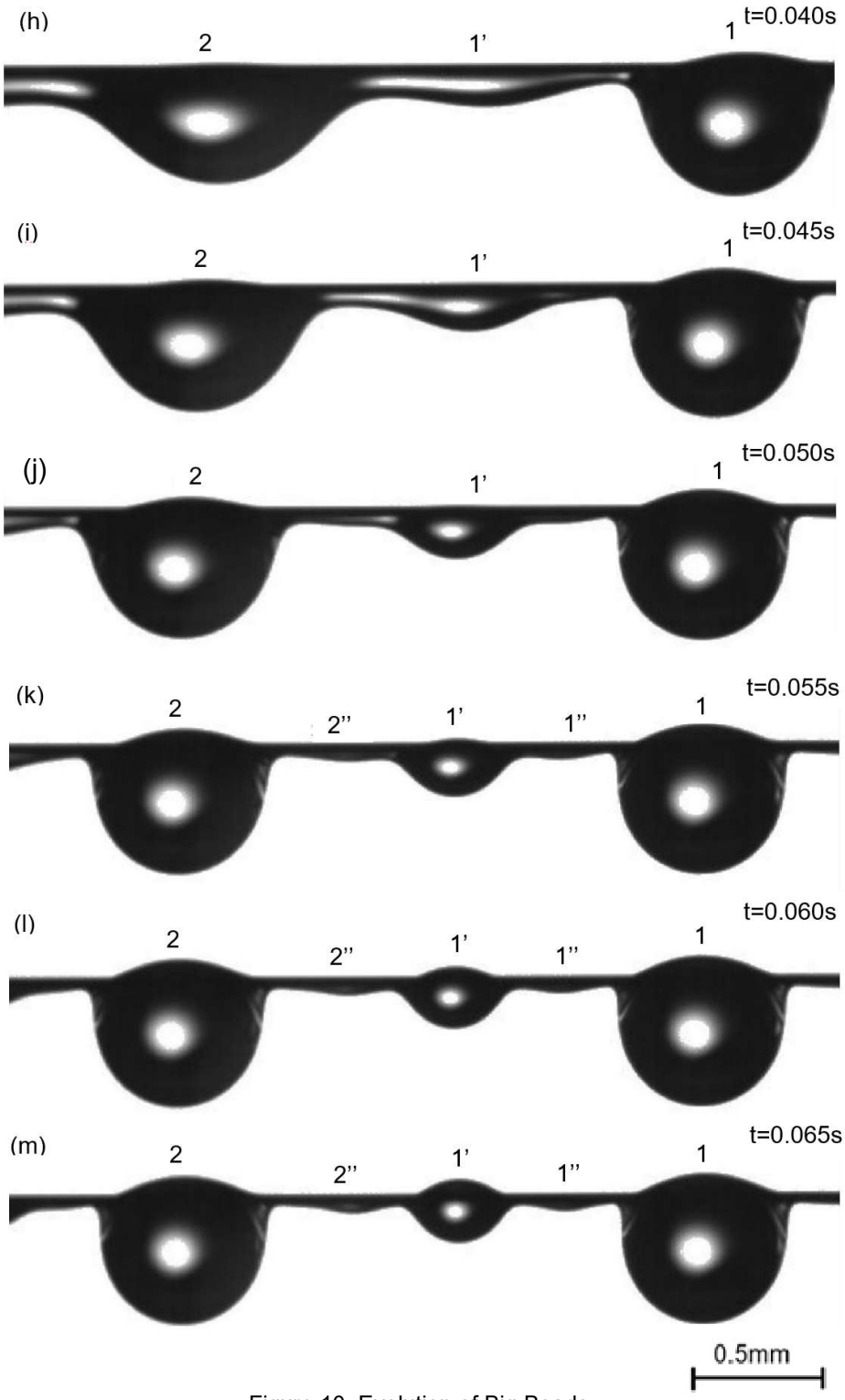

Figure 10: Evolution of Big Beads

(i) In the above case, we achieved large beads by horizontal drawing of the fiber from the fluid reservoir at a velocity of 35 cm/s.

(ii) The figure 10(a) shows the silicone oil fluid film coating over the fiber which is made to halt at *t*=0.000s.

(iii) Figures 10(b), 10(c) & 10(d) show the primary and secondary beads to occur by the pinching of the neck that leads to the film separation into droplets of silicone oil over copper wire.

(iv) This neck region created between the primary and secondary bead gets thinner with every time step until the film breaks separate as that seen in figure 10(g), at *t*=0.035s.

(v) Beads in figure 10(h) &10(i) grow into a full bead of a spherical shape. Simultaneously, the *satellite bead* 1' is formed between the primary and secondary beads, as seen in figure 10(j) at *t*=0.050s.

(vi) By the next time step, *t*=0.055s, there is still some left-over fluid film that recoils and feeds to again form on either side of the *satellite beads*. These are the 1''and 2'' beads which are named as the '*sub-satellite beads'*. These beads are too small, approximately less to the size of small beads.

(vii) Figures 10(k) to 10(m) portrays all the three kinds of beads, i.e., primary and secondary beads, *satellite beads* and the *sub-satellite beads*.

Note: All the three figures (8, 9 &10) have the magnitude scale mentioned at the bottom right of the last picture.

5.4 Experimental Data:

5.4.1 Small Beads

$v=d/t$=5.785/0.175=3.3 cm/s				
bead #	H_1 (mm)	L (mm)	θ (deg)	λ^* (mm)
1	0.16	0.33	24.00	
				0.57
2	0.15	0.33	22.00	
				0.54
3	0.14	0.28	25.00	
				0.43
4	0.13	0.28	18.00	
Avg. value	0.14	0.31	22.25	0.51

Table 1: Small Beads Trial 1

$v=d/t$=6.180/0.195=3.169cm/s				
bead #	H_1 (mm)	L (mm)	θ (deg)	λ^* (mm)
1	0.16	0.33	25.00	
				0.64
2	0.16	0.32	21.00	
				0.79
3	0.17	0.34	24.00	
				0.66
4	0.15	0.32	23.30	
Avg. value	0.16	0.33	23.33	0.70

Table 2: Small Beads Trial 2

$v=d/t$=5.927/0.13=4.5 cm/s				
bead #	H_1 (mm)	L (mm)	θ (deg)	λ^* (mm)
1	0.19	0.38	25.00	
				0.68
2	0.17	0.36	24.00	
				0.59
3	0.16	0.32	25.00	
				0.59
4	0.16	0.35	30.00	
Avg. value	0.17	0.35	26.00	0.62

Table 3: Small Beads Trial 3

5.4.2 Medium Beads

$v=d/t$=8.316/0.049=16.97 cm/s				
bead #	H_1 (mm)	L (mm)	θ (deg)	λ^* (mm)
1	0.44	0.68	37.00	
				1.48
2	0.48	0.72	41.00	
				1.78
3	0.50	0.77	40.00	
Avg. value	0.47	0.72	39.33	1.63

Table 4: Medium Beads Trial 1

$v=d/t$=9.212/0.043=21.4 cm/s				
bead #	H_1 (mm)	L (mm)	θ (deg)	λ^* (mm)
1	0.75	0.94	39.00	
				2.23
2	0.78	1.01	39.00	
				2.40
3	0.86	1.09	37.80	
Avg. value	0.80	1.01	38.60	2.32

Table 5: Medium Beads Trial 2

$v=d/t$=8.961/0.048=18.668 cm/s				
bead #	H_1 (mm)	L (mm)	θ (deg)	λ^* (mm)
1	0.56	0.84	41.00	
				2.50
2	0.54	0.79	37.00	
				2.15
3	0.59	0.84	39.00	
Avg. value	0.56	0.82	39.00	2.32

Table 6: Medium Beads Trial 3

5.4.3 Big Beads

$v=d/t$=8.678/0.022=39.45cm/s				
bead #	H_1 (mm)	L (mm)	θ (deg)	λ^* (mm)
1	0.95	1.11	26.00	3.66
2	0.96	1.11	32.00	
Avg. value	0.96	1.11	29.00	3.66

Table 7: Big Beads Trial 1

$v=d/t$=7.72/0.021=36.76cm/s				
bead #	H_1 (mm)	L (mm)	θ (deg)	λ^* (mm)
1	0.91	1.06	24.40	2.93
2	0.99	1.13	25.30	
Avg. value	0.95	1.10	24.85	2.93

Table 8: Big Beads Trial 2

5.5 Graphs

The following graph is the theoretical graph, taken between the Volume of the bead, *V* and the Radius of Curvature of the bead, *R*.

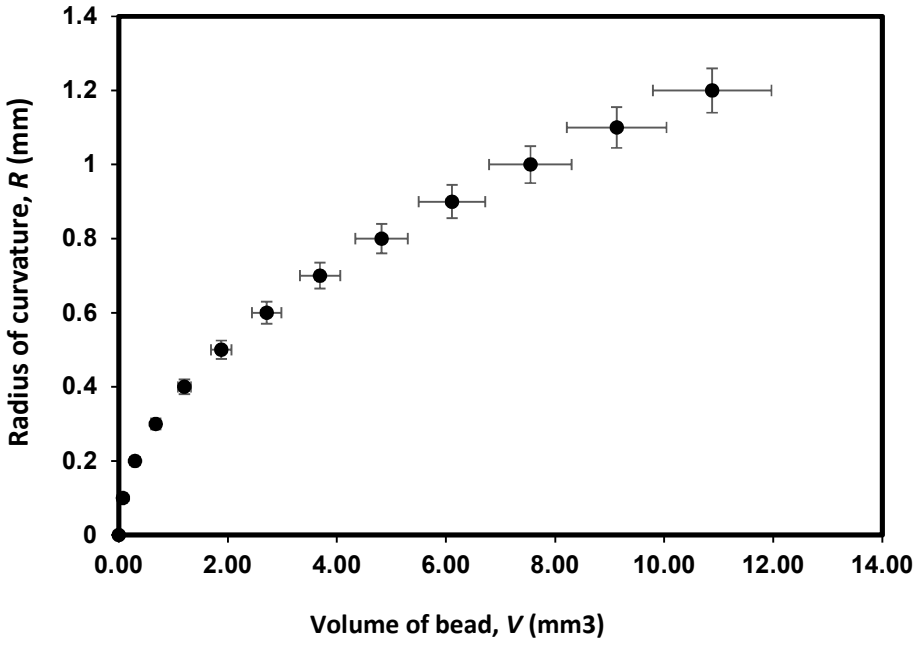

Figure 11: Theoretical graph *V* vs *R*

The following two graphs consists of the averaged values of the fiber withdrawal velocity, lengths and heights of the beads from the trial experiments as shown in the tables (1-8).

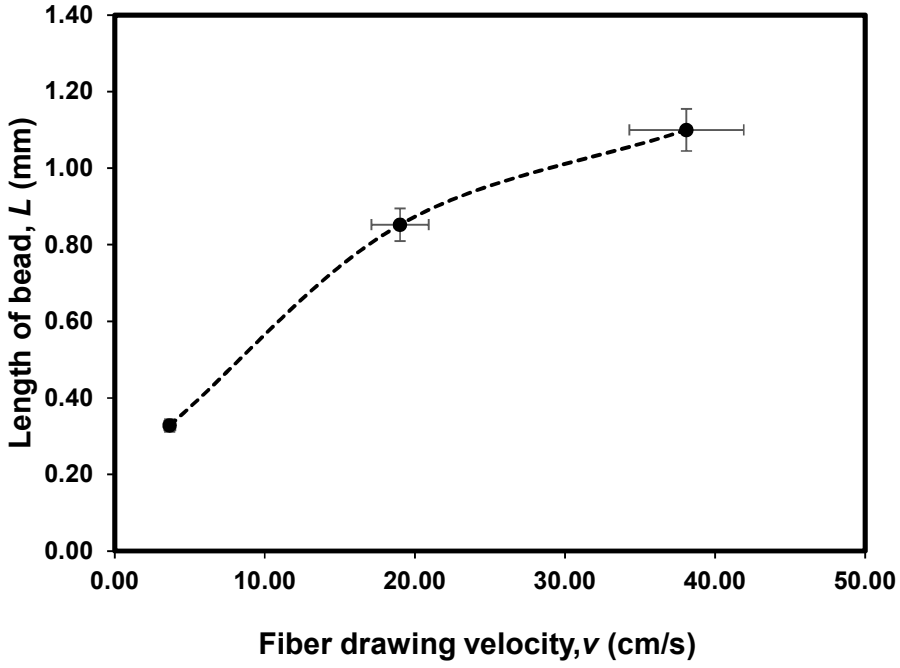

Figure 12: Average *v* vs *L* graph

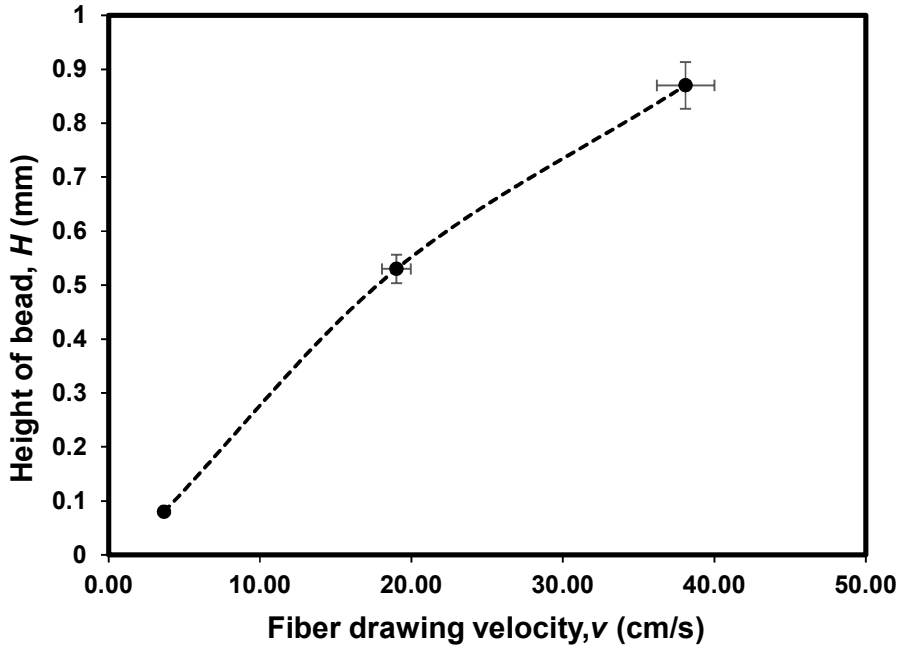

Figure 13: Average *v* vs *H* graph

5.6 Theoretical & Experimental Comparison

Beads	v (cm/s)	R (mm)	θ (deg)	L_{th} (mm)	H_{th} (mm)	L_{exp} (mm)	H_{exp} (mm)
Small	3.50	0.29	20.00	0.20	0.02	0.28	0.08
Medium	16.00	0.62	36.50	0.73	0.12	1.05	0.72
Big	35.00	0.91	25.00	0.77	0.09	1.14	0.96

Table 9: Bead Geometrical Data

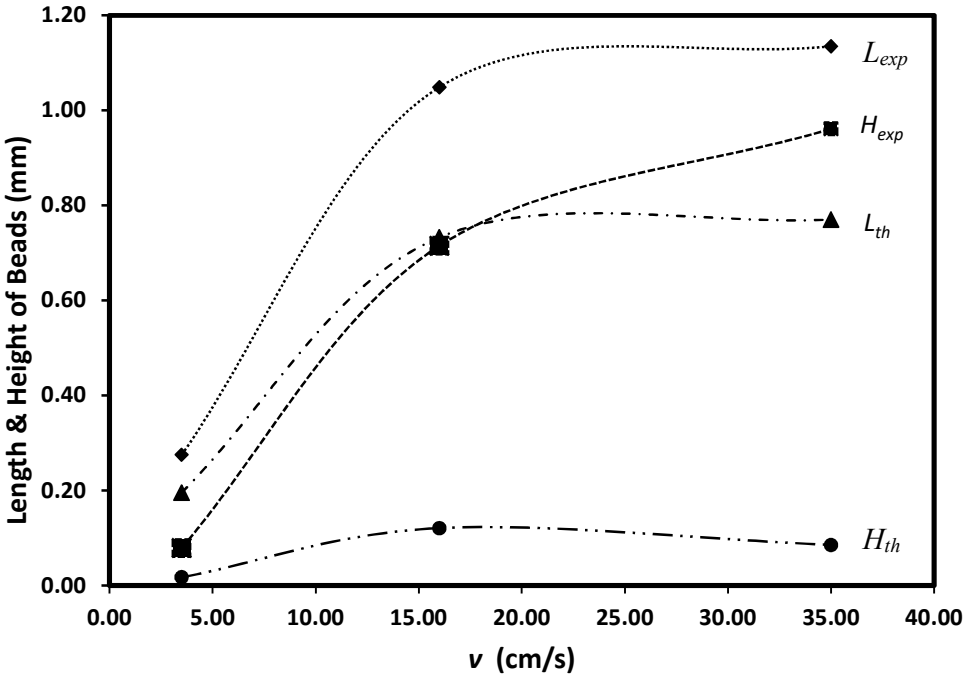

Figure 14: Theoretical & Experimental Data Comparison

(i) Above data is of the silicone oil beads over copper wire.

(ii) R, θ and v were measured directly from the video using the analysis software to briefly understand the variation of the experimental curve with the theoretical curve for v vs. L *and* v vs. H graphs.

Description

The graph is plotted between the fiber drawing velocity, *v* (cm/s) and the bead data that includes the length of the bead (mm) and height of the bead (mm) of both the theoretical and experimental values respectively. For theoretical calculation we use the equations (4) and (5) from the mathematical model section and for the experimental values we directly measure the length and height of the beads from the experiment. This would give two curves for both *v* vs. *L* and *v* vs. *H* respectively, i.e., theoretical and experimental curves.

Observation

The experimental curves of both *v* vs. *L* and *v* vs. *H* are higher than their theoretical curves respectively because the theoretical values are applicable only for small beads. Hence, as the bead sizes increases, the data deviates with the theory.

5.7 Solid Bead Fabrication

The fabrication setup used in this work is used for the experiment to produce solid beads. Here, we use nylon fiber that is horizontally drawn from a polymer solution reservoir, consisting of PMMA (Polymethylmethacrylate)/DMF (N, N Dimethylformamide), with a weight percentage of 11%, two capillary tubes are fixed to the walls of the solution container to guide the fiber. The fiber is drawn-out steadily from the solution reservoir using pulley 'B' (as seen in fig 7) to achieve fluid coating over the fiber. The DMF component evaporates to give PMMA solid beads on the fiber. This shall be used for stroke-study application.

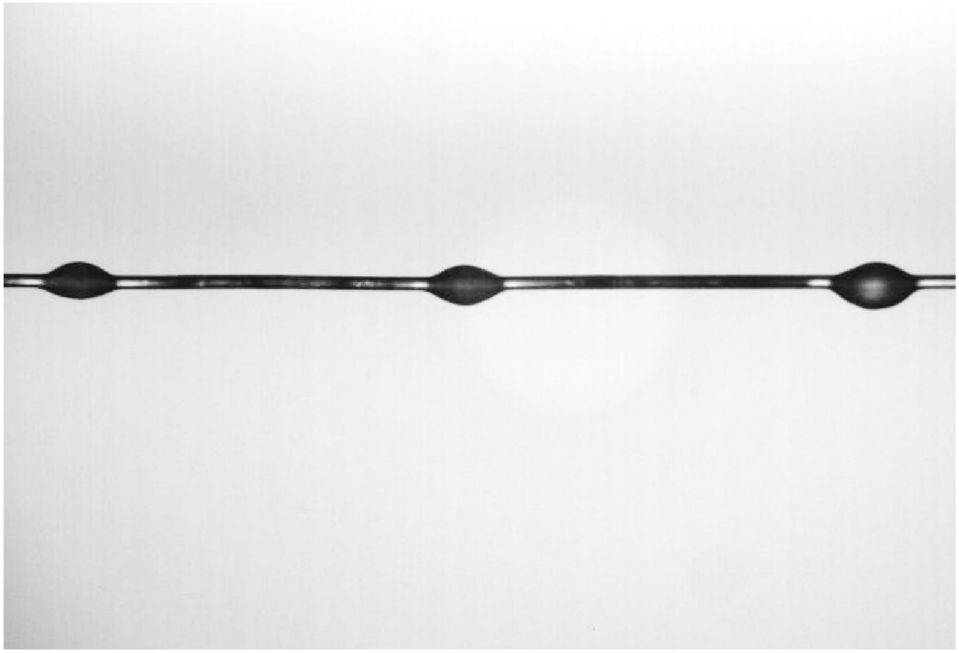

Figure 15: Solid beads on fiber

5.8 Conclusions

(i) The current research shows the relation between the velocity of fiber drawn, *v*, and the length of the beads on fiber, *L*, to be increasing with increase in the velocity. Similar scenario is seen in the case of *v* vs *H* graphs.

(ii) By controlling the velocity, we achieved same sized beads-on-fiber at regular intervals.

(iii) This work also provides an experimental approach to produce solid beads on fiber.

5.9 Future Work

5.9.1 Solid Beads Mass Fabrication

Further studies on understanding the challenges of solid beads on fiber can be carried out.

5.9.2 Vertical Fiber Withdrawal

Vertical fiber withdrawal from liquid reservoir can also be experimented to further study the formation of beads on fiber. In this case the gravitational force will also be considered, hence the affect of gravity on beads-on-fiber can be an interesting case of study.

5.9.3 Comparison study

Different fluids and fiber combinations can be studied. Comparative study can be carried out to understand the bead behavior on various fibers for future applications purposes.

Chapter 6 CITATIONS

(1) Bai, H.; Sun, R.; Ju, J.; Yao, X.; Zheng, Y.; Jiang, L. Large-Scale Fabrication of Bioinspired Fibers for Directional Water Collection. *Small* **2011**.

(2) Gao, F.; Sonin, A. A. Precise Deposition of Molten Microdrops: The Physics of Digital Microfabrication. *Proc. R. Soc. A Math. Phys. Eng. Sci.* **1994**, *444* (1922), 533–554.

(3) SCHIAFFINO, S.; SONIN, A. A. Formation and Stability of Liquid and Molten Beads on a Solid Surface. *J. Fluid Mech.* **1997**, *343*, S0022112097005831.

(4) Quéré, D. FLUID COATING ON A FIBER. *Annu. Rev. Fluid Mech.* **1999**, *31* (1), 347–384.

(5) Isenberg, C. Soap Films and Bubbles. *Phys. Educ.* **1981**, *16* (4), 218–222.

(6) Carroll, B. J. The Accurate Measurement of Contact Angle, Phase Contact Areas, Drop Volume, and Laplace Excess Pressure in Drop-on-Fiber Systems. *J. Colloid Interface Sci.* **1976**.

(7) Plateau, J. Experimental and Theoretical Statics of Liquids Subject to Molecular Forces Only. *Gauthier-Villars, Paris* **1873**.

(8) de Gennes, P.-G.; Brochard-Wyart, F.; Quéré, D. *Capillarity and Wetting Phenomena*; 2004.

(9) Brinker, C. J.; Frye, G. C.; Hurd, A. J.; Ashley, C. S. Fundamentals of Sol-Gel Dip Coating. *Thin Solid Films* **1991**, *201* (1), 97–108.

(10) Oliveira, M. S. N.; McKinley, G. H. Iterated Stretching and Multiple Beads-on-a-String Phenomena in Dilute Solutions of Highly Extensible Flexible Polymers. *Phys. Fluids* **2005**, *17* (7), 1–4.

(11) Luo, C. Theoretical Exploration of Barrel-Shaped Drops on Cactus Spines. *Langmuir* **2015**, *31* (43), 11809–11813.

(12) Partenhauser, A.; Laffleur, F.; Rohrer, J.; Bernkop-Schnch, A. Thiolated Silicone Oil: Synthesis, Gelling and Mucoadhesive Properties. *Acta Biomater.* **2015**, *16* (1), 169–177.

Biographical Information

Kirthika Suresh is pursuing her Master's Degree in Mechanical Engineering at the University of Texas at Arlington and holds a Bachelor's Degree in Aerospace Engineering from SRM University, Kattankulathur, India in 2016.

She works in Micro/Nano Systems Lab as a part of Dr. Cheng Luo's group. During her study she carried out experiments relating to beads on fiber, Leidenfrost study over parallel channels, ratchets and plates.

Her focus of study is on 'Mass Fabrication and Evolution of Beads on Fiber'. She is very keen on applying her knowledge in the Mechanical and Aerospace industries. She would also like to pursue Doctor of Philosophy in the future.